

## Supporting Information

### **Halloysite-derived mesoporous silica with high ionic conductivity improves Li-S battery performance**

Ranxiao Ao<sup>a</sup>, Ziqi Zhu<sup>a</sup>, Shilin Zhang<sup>b, c</sup>, Qiang Zhang<sup>b, c</sup>, Chenyu Yan<sup>a</sup>, Feiyue Tu<sup>d</sup>, Tianbao Li<sup>d</sup>,

Mitch Guijun Li<sup>e</sup>, Liangjie Fu<sup>a, b, c \*</sup>, Aidong Tang<sup>a, b, c \*</sup>, Huaming Yang<sup>a, b, c \*</sup>

<sup>a</sup> *Engineering Research Center of Nano-Geomaterials of Ministry of Education, Laboratory of Advanced Mineral Materials, Faculty of Materials Science and Chemistry, China University of Geosciences, Wuhan 430074, China*

<sup>b</sup> *College of Chemistry and Chemical Engineering, Central South University, Changsha 410083, China*

<sup>c</sup> *Hunan Key Laboratory of Mineral Materials and Application, School of Minerals Processing and Bioengineering, Central South University, Changsha 410083, China*

<sup>d</sup> *Changsha Research Institute of Mining and Metallurgy Co. LTD. Changsha 410012, P. R. China*

<sup>e</sup> *Division of Integrative Systems and Design, Department of Electronic and Computer Engineering, The Hong Kong University of Science and Technology, Clear Water Bay, Kowloon, Hong Kong SAR, P. R. China*

\*Corresponding author

E-mail: tangaidong@cug.edu.cn; adtang@csu.edu.cn (A. Tang);  
hm.yang@cug.edu.cn; hmyang@csu.edu.cn (H. Yang); [franch@cug.edu.cn](mailto:franch@cug.edu.cn) (L. Fu)

## Experimental Section

### Chemicals and Instrumentations

The acquisition of unprocessed halloysite is purchased from Sigma-Aldrich (Shanghai) Co., Ltd. Commercial sulfur powder, N-methyl-2-pyrrolidone (NMP), and poly (ethylene oxide)-block-poly (propylene oxide)-block-poly (ethylene oxide) triblock copolymer ( $M_{avg.} = 5800$ , P<sub>123</sub>) and polyvinylidene difluoride (PVDF) were acquired from Shanghai Aladdin Bio-Chem Technology Co., Ltd, located in China. Acetylene black, Ferric nitrate nine-hydrate, hydrochloric acid (HCl) and sodium hydroxide (NaOH) were obtained from Sinopharm Chemical Reagent Co., Ltd, China. All reagents were utilized without undergoing additional purification. For all the experiments, ultrapure water (Millipore, 18.25 M $\Omega$  cm<sup>-1</sup>) was utilized.

### Instrumentations

Wide-angle X-ray diffraction (WAXRD, Bruker D8 advance) with Cu K $\alpha$  radiation characterized the crystal structures of the samples in the  $2\theta$  range of 5° to 80°. Scanning electron microscopy (SEM, FEI nanoSEM450) and transmission electron microscopy (TEM, Jem-2100F) were used to test the morphologies of the samples. The specific surface areas were determined using nitrogen adsorption measurements at a temperature of 77 K, employing a Micromeritics ASAP 2460 plus gas adsorption apparatus. The multipoint Brunauer-Emmett-Teller (BET) method was used to calculate the specific surface areas. The total pore volumes ( $V_{tot}$ ) are calculated based on the volumes of adsorbed gas at a relative pressure ( $P/P_0$ ) of 0.995. The pore size distributions are derived from the adsorption branches of the acquired isotherms by the utilization of the Barrett-Joyner-Halenda (BJH) method. The sample's elemental

chemical environment was characterized using X-ray photoelectron spectroscopy (XPS, Thermofisher escalab 250xi). The samples were characterized for their elemental composition and content using inductively coupled plasma emission mass spectrometry (ICP, ICAP-QC). The high-resolution solid-state NMR spectra of the samples were measured by the dipole decoupling magic Angle rotating NMR method (Bruker 400M) at MAS spin rate of 10 KHz.

### **Synthesis of HSBA-15**

Typically, 5 g of raw halloysite was subjected to treatment 250 mL of 6 mol L<sup>-1</sup> HCl under stirring for 6 h at 100 °C in oil-bath. Next, dissolved the dried solid product in 2 mol L<sup>-1</sup> NaOH under magnetic stirring for 6 h at 50 °C, and the resulting solution of sodium silicate was then prepared for standby by centrifuging. After 1 g of P<sub>123</sub> embedded co-polymer is mixed and dissolved in a solution of 30 mL HCl (2mol L<sup>-1</sup>) for 20 hours, add 5 mL of Sodium halloysite solution and continue to stir for 24 hours. The P<sub>123</sub> solution is transferred into a polypropylene vial and heated at 100 °C for 48 h. Wait for the mixture to cool to room temperature and recycle the precursor by filtering and washing and drying at 50 °C in a vacuum cooker. The precursor is then heated in the furnace at 5°C min<sup>-1</sup> to 550°C for 2 hours to obtain silicon dioxide (HSBA-15).

### **Synthesis of Fe-HSBA-15**

0.5g of mesoporous silica and ferric nitrate were magnetically stirred in 60ml of ethanol at a certain mass ratio for 24 hours. After stirring evenly, the solid product is obtained by centrifugation, and the solid product is freeze-dried. The precursor is then heated in the furnace at 5°C min<sup>-1</sup> to 550°C for 2 hours to obtain Fe-HSBA-15.

### **Synthesis of Fe-HSBA-15/S**

Fe-HSBA-15 and sulfur were thoroughly combined in a 1:4 mass ratio and thereafter

subjected to heating at 155 °C for a duration of 12 h in an argon environment. After cooling down, the agglomerated composition was grinded for 30 min to synthesize Fe-HSBA-15/S. The same method is also used for the fabrication of the reference samples.

### **Electrochemical measurements**

All Li-S battery tests were carried out by standard 2016-type coin cells. Typical, the slurry was made via uniform mixing Fe-HSBA-15/S, acetylene black and PVDF (7:2:1). Subsequently, the slurry was applied onto an aluminum foil that had been previously coated with carbon. The coin cells were assembled with lithium metal as a counter electrode and polypropylene membrane as the separator, and the electrolyte was 1.0 M Li bis (tri-flu-omethanesulphonyl) imide (LiTFSI) dissolved in 1, 3 dioxolane (DOL) and 1, 2-dimethoxyethane (DME) (1:1 by volume) with 1.0 wt.% LiNO<sub>3</sub> as additive. The batteries were built within a glovebox that contained ultra-pure Ar gas, ensuring that the levels of water and oxygen remained below 0.01 p.p.m. The galvanostatic charge-discharge experiments were performed at a temperature of 25 °C using a Land battery tester (Land CT3001A, China) at various rates within the voltage range of 1.5-2.8 V. Cyclic voltammetry (CV) was conducted utilizing an electrochemical workstation (CHI760E Shanghai, China). The specific capacity is determined by the mass of Sulphur (S) present in the active material, while the areal sulfur loading is approximately 1.5~2 mg cm<sup>-2</sup>.

### **Evaluation of ionic transferring kinetics**

Fe-HSBA-15 and PVDF were thoroughly combined in a 1:1 mass ratio, and the slurry was applied onto a glass plate, vacuum drying at 80°C for 12 h. The ionic conductivity was tested *via* an EIS method on the electrochemical working station with the frequency range from 10<sup>-1</sup>-10<sup>6</sup> Hz. The ionic conductor membranes were sandwiched between two pieces of stainless steel (as blocking electrodes). The ionic

conductivity was calculated according to the equation of  $\sigma = L / (R \times S)$ . Where  $\sigma$  is the ionic conductivity ( $\text{S cm}^{-1}$ ),  $L$  is the thickness of the membrane (cm),  $S$  is the area of the membrane or tablet ( $\text{cm}^2$ ) (this work: the  $L$  values of PVDF, HSBA-15 and Fe-HSBA-15 are determined to be  $2.1 \times 10^{-4}$ ,  $1.1 \times 10^{-4}$ ,  $2.8 \times 10^{-4}$  cm, respectively.  $S=0.785 \text{ cm}^2$ ), and  $R$  is the bulk resistance ( $\Omega$ ).

### **Lithium-ion transference number**

The lithium-ion transference number ( $t_{\text{Li}^+}$ ) was evaluated via the chronoamperometry and EIS methods with assembled lithium symmetric battery (Li | ionic conductor membrane | Li) at room temperature. The  $t_{\text{Li}^+}$  can be calculated by the equation of

$$t_{\text{Li}^+} = I_{\text{ss}} (\Delta V - I_0 \times R_0) / I_0 (\Delta V - I_{\text{ss}} \times R_{\text{ss}})$$

where the direct current polarization voltage ( $\Delta V$ ) is 10 mV,  $R_0$  and  $R_{\text{ss}}$  are the impedances before and after polarization, and  $I_0$  and  $I_{\text{ss}}$  are the initial and stable currents during polarization.

### **Theoretical Calculations**

The calculations were performed using the CASTEP (Cambridge Sequential Total Energy Package) code, employing the Perdew, Burke, and Ernzerhof (PBE)<sup>1</sup> exchange-correlation potential and the Grimme (PBE-D2) van der Waals corrections.<sup>2</sup> The cutoff energy utilized is 500 eV, employing the ultrasoft pseudo-potential plane-wave formalism and density-mixing technique.<sup>3</sup> A  $2 \times 2 \times 1$  Monkhorst-Pack k points mesh was employed for doing electrical structure calculations, whereas the Gamma point was utilized for conducting geometrical calculations. The convergence requirements for the self-consistent field (SCF) tolerance were set at  $1.0 \times 10^{-6}$  eV. The silica surface structure  $\text{Si}_{27}\text{O}_{36}(\text{OH})_{36}$  is formed by introducing a 25 Å vacuum in (0 0 1) direction after

cleaving the 3×3×3 bulk silica structure. The silica surface is passivated by H atoms to simulate the hydroxylated silica surface. The c-axis remains stationary during the relaxing process. The atomic position and cell parameters of all structures underwent complete relaxation using the Broyden-Fletcher-Goldfarb-Shanno (BFGS) minimization algorithm. The Li<sub>2</sub>S<sub>x</sub> cluster formations are contained within a 20 Å box. The initial adsorption configurations of Li<sub>2</sub>S<sub>x</sub> species on the silica surface were determined by Grand Canonical Monte Carlo (GCMC) simulations using the Adsorption Locator module of Materials Studio software. The Universal force field was utilized, with the charges of the atoms determined by DFT calculations. After then, the Li<sub>2</sub>S<sub>x</sub>/silica interface structures were further relaxed by DFT calculations. The binding energy of Li<sub>2</sub>S<sub>x</sub> was calculated by  $E_{\text{ads}}=E_{(\text{mix})}-E_{(\text{Fe/SiO}_2)}-E_{(\text{Li}_2\text{S}_x)}$ . The  $E_{\text{mix}}$  is the entire energy of the adsorption system (eV),  $E_{\text{Fe/SiO}_2}$  stands for the energy of SiO<sub>2</sub> structural units (eV),  $E_{(\text{Li}_2\text{S}_x)}$  represents the energy of Li<sub>2</sub>S<sub>x</sub> surfaces (eV). A negative  $E_{\text{ads}}$  mean that the Li<sub>2</sub>S<sub>x</sub> can be adsorbed on the SiO<sub>2</sub>.

## Supporting figures

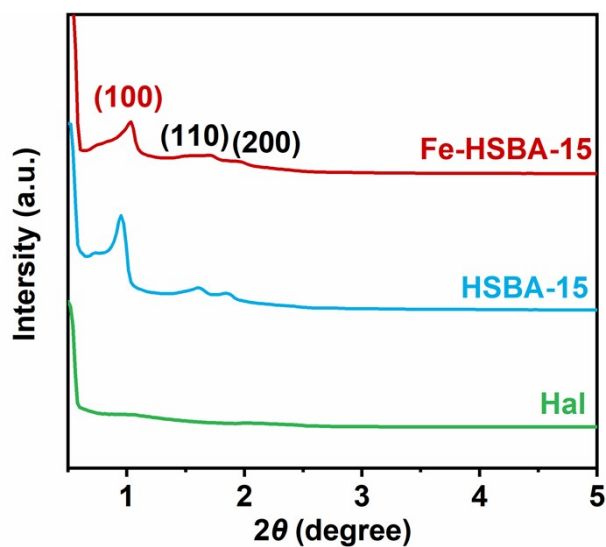


Fig. S1. SAXRD patterns of halloysite, HSBA-15 and Fe-HSBA-15

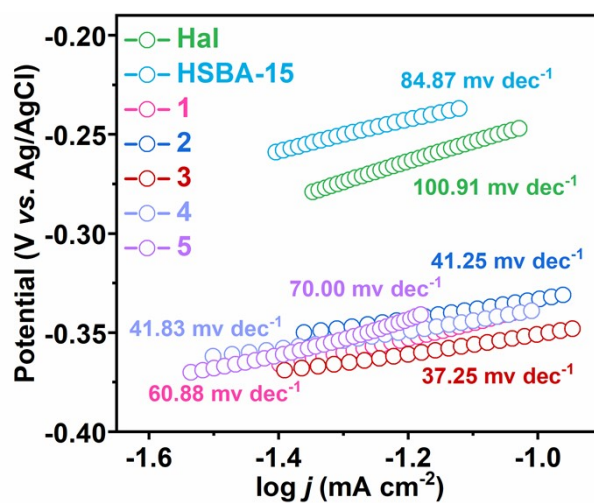
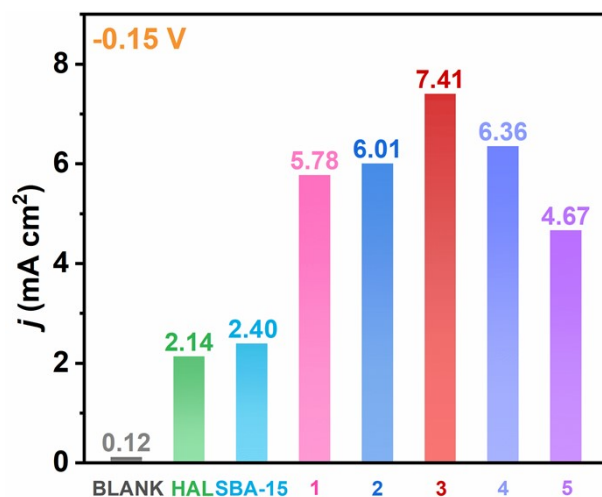
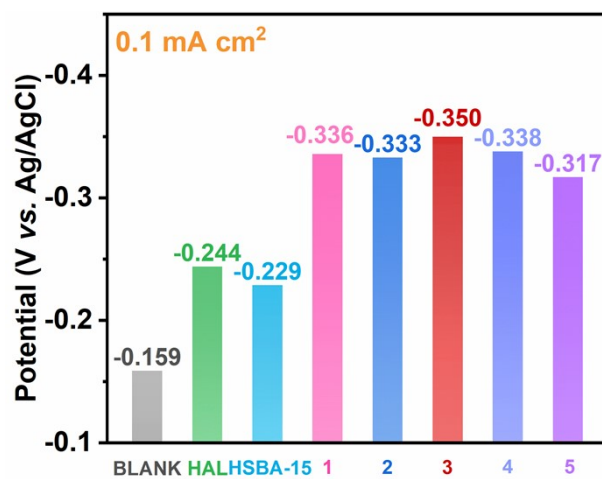


Fig. S2. Tafel slope of halloysite, HSBA-15 and Fe-HSBA-15.



**Fig. S3.** Current density of halloysite, HSBA-15 and different ratios of Fe-HSBA-15 at -0.15 V.



**Fig. S4.** Initial potential of halloysite, HSBA-15 and different ratios of Fe-HSBA-15 at 0.1 mA cm<sup>2</sup>.

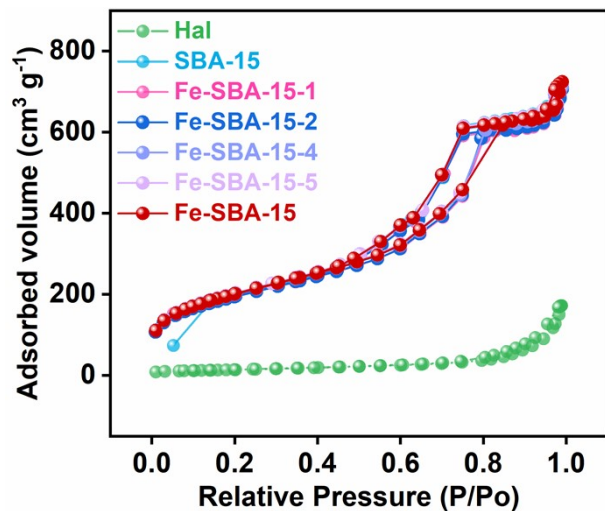


Fig. S5. Nitrogen adsorption-desorption isotherms of halloysite, HSBA-15 and Fe-HSBA-15.

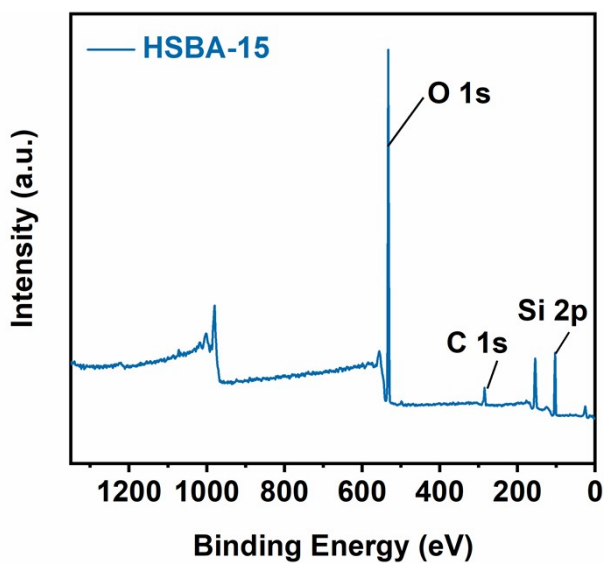


Fig. S6. XPS survey spectrum of HSBA-15.

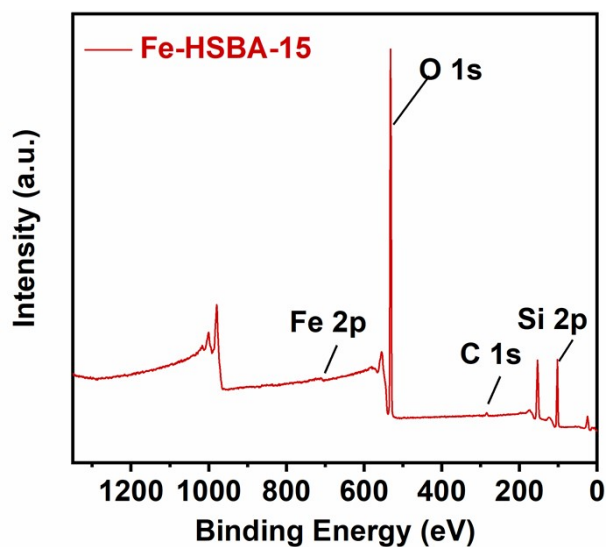


Fig. S7. XPS survey spectrum of Fe-HSBA-15.

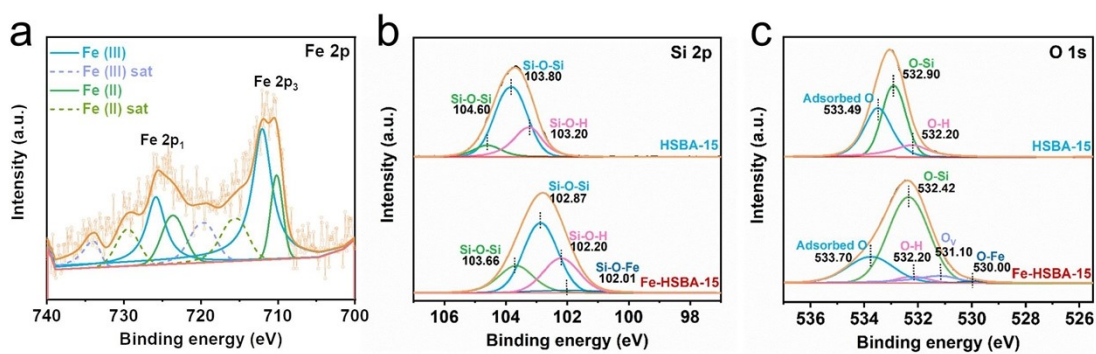


Fig. S8. XPS spectra of (a) Fe 2p, (b) Si 2p, (c) O1s.

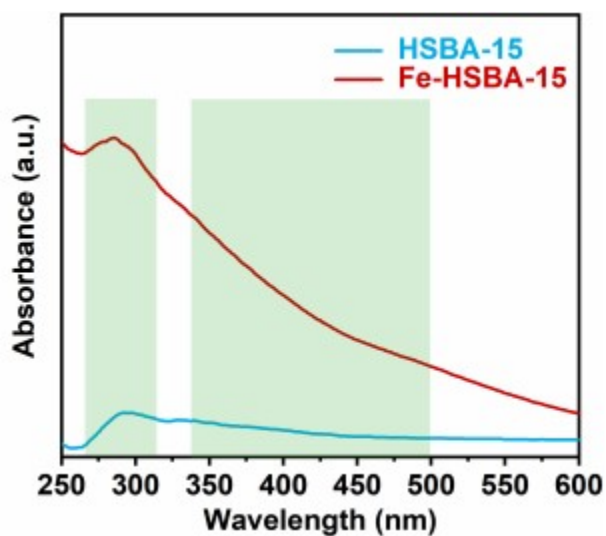
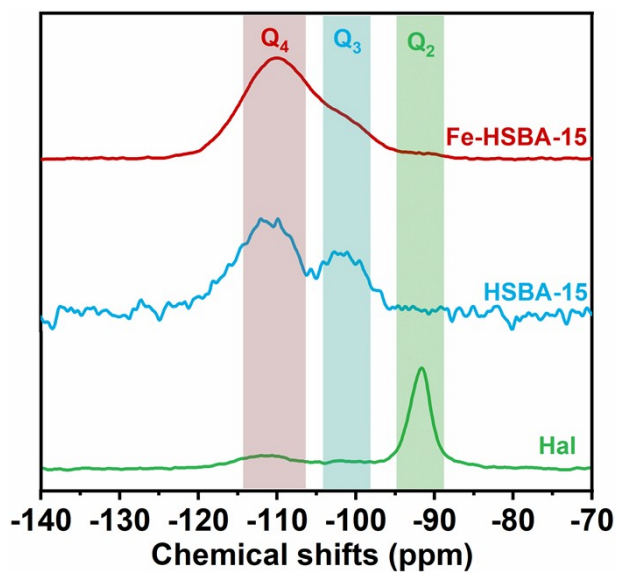
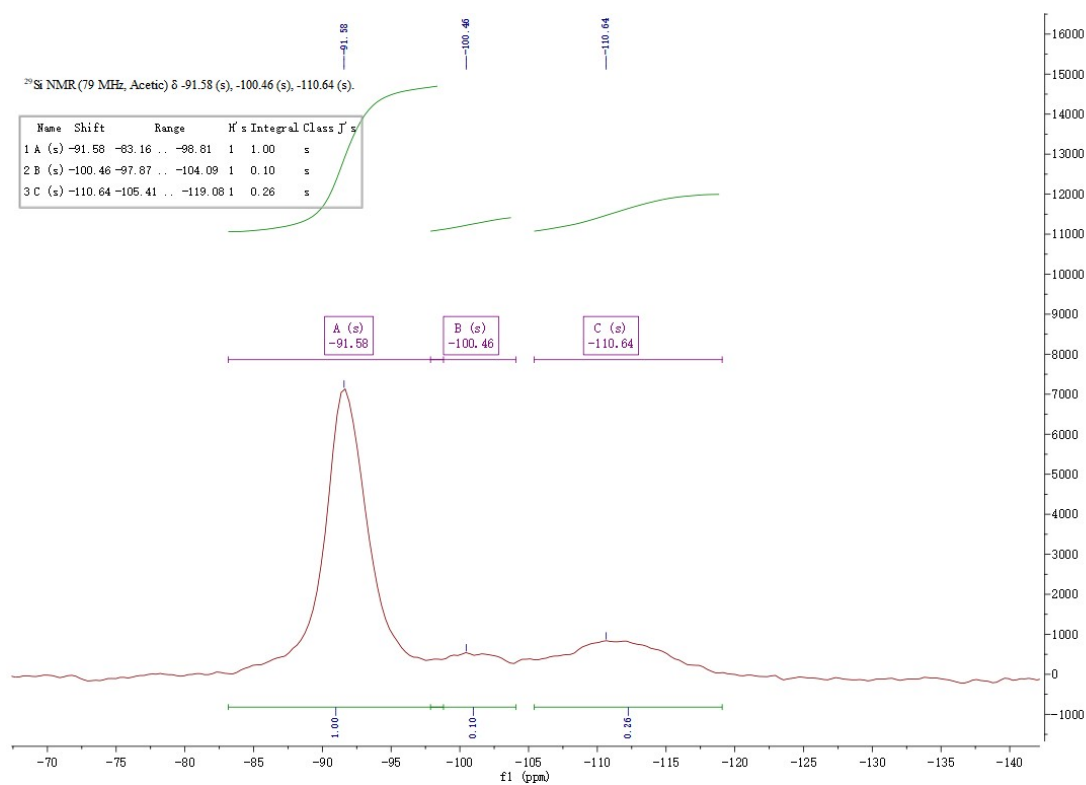


Fig. S9. UV-Vis DRS spectra of Fe-HSBA-15 and HSBA-15.



**Fig. S10.** Si MAS NMR spectrum of halloisite, HSBA-15 and Fe-HSBA-15.



**Fig. S11.** NMR spectrum of halloisite.

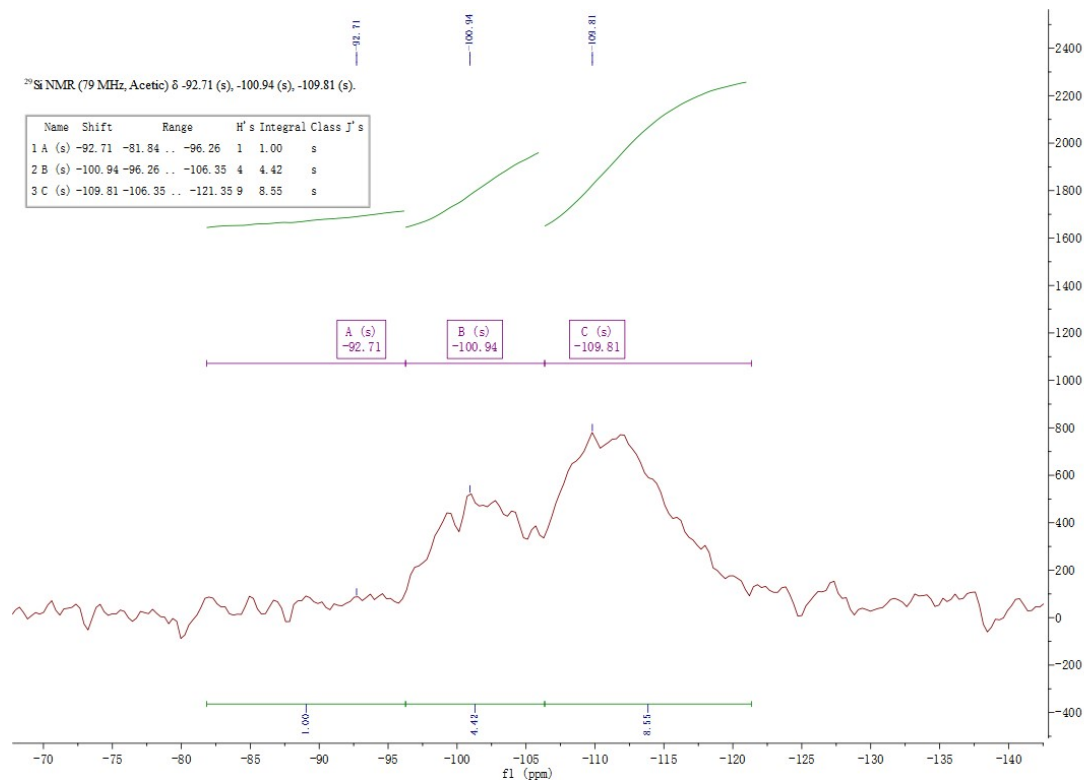


**Fig. S12.** NMR spectrum of HSBA-15.

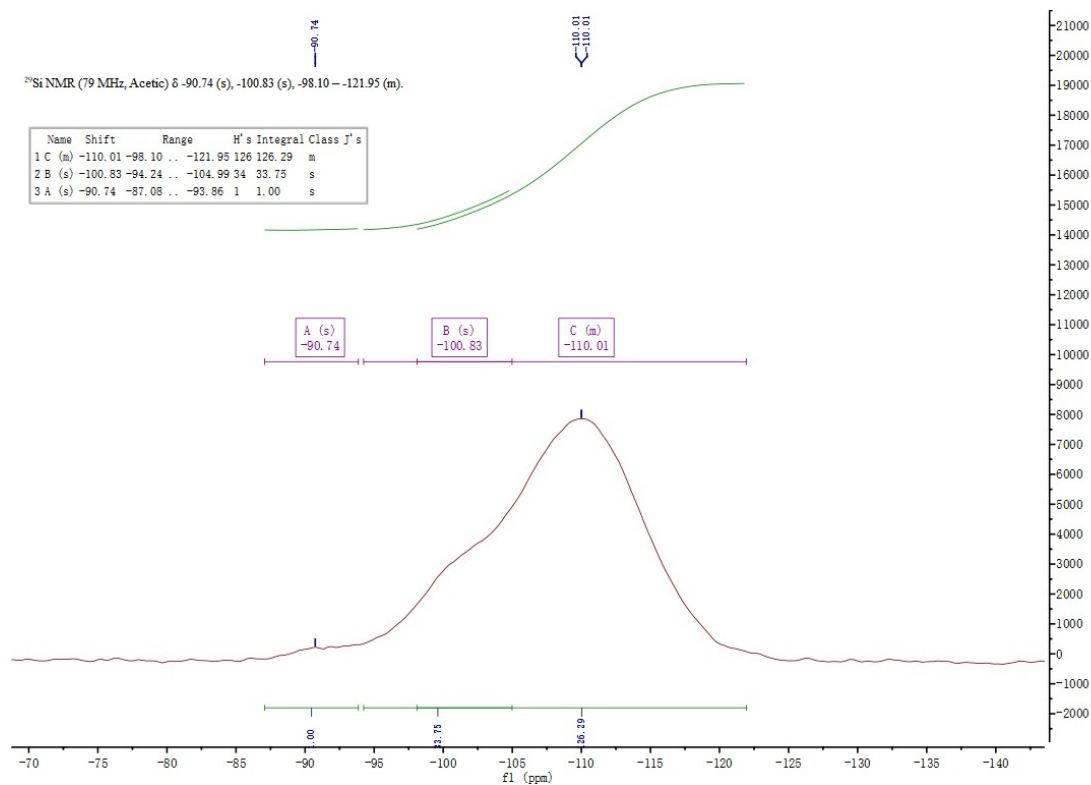


**Fig. S13.** NMR spectrum of Fe-HSBA-15.

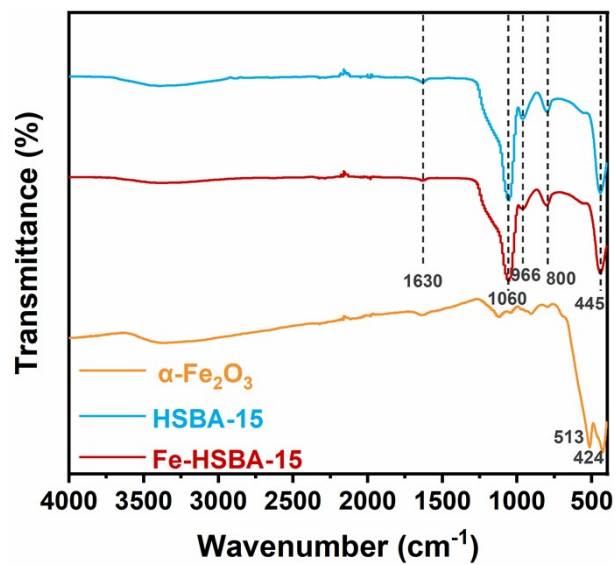


**Fig. S14.** FTIR spectra of  $\alpha$ -Fe<sub>2</sub>O<sub>3</sub>, Fe-HSBA-15 and HSBA-15.

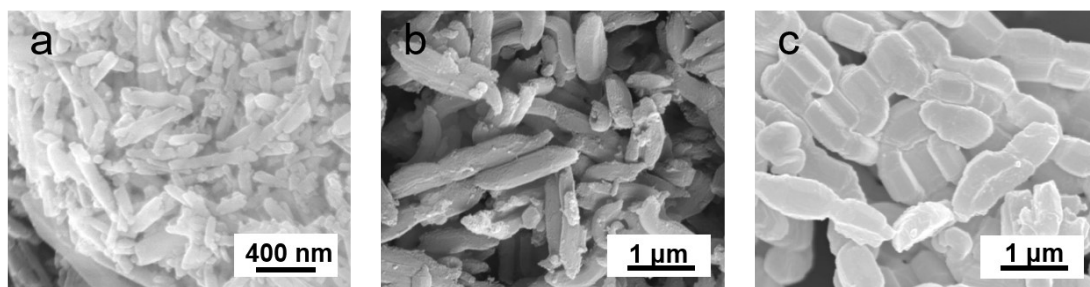


**Fig. S15.** SEM images of halloysite (a), HSBA-15 (b) and Fe-HSBA-15 (c).

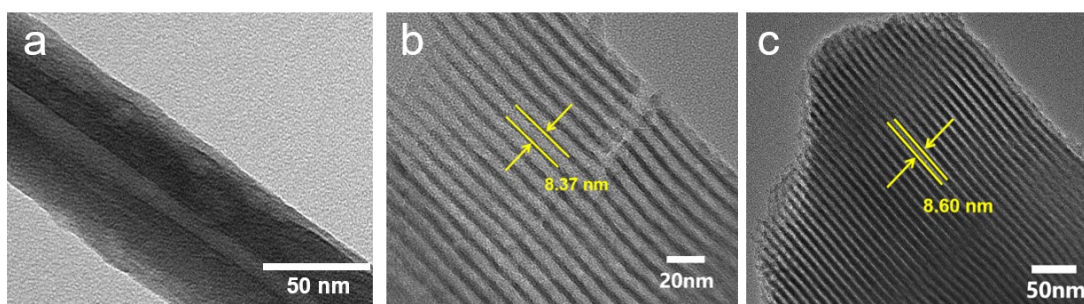


**Fig. S16.** TEM images of halloysite (a), HSBA-15 (b) and Fe-HSBA-15 (c).

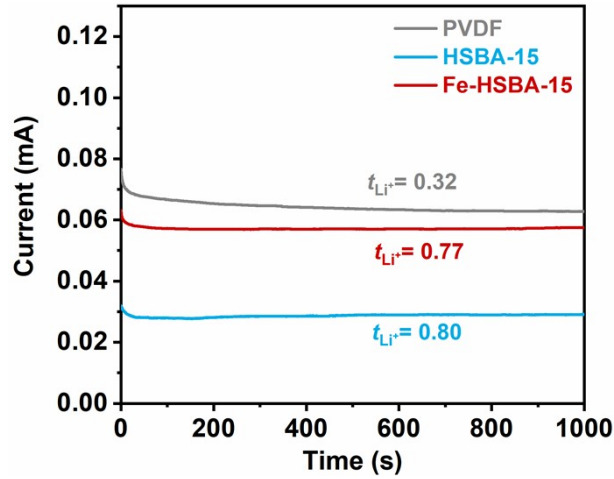


**Fig. S17.**  $\text{Li}^+$  transference numbers of Fe-HSBA-15 and PVDF ionic conductor membrane.

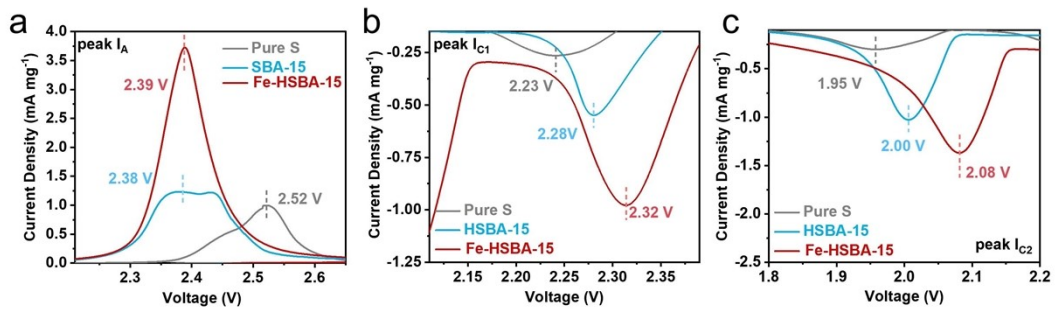


**Fig. S18.** CV curves (a) of an enlarged view in (b) peak  $I_A$  and (c) peak  $I_{C1}$  and (d) peak  $I_{C2}$  of Li-S batteries with different carrier materials.

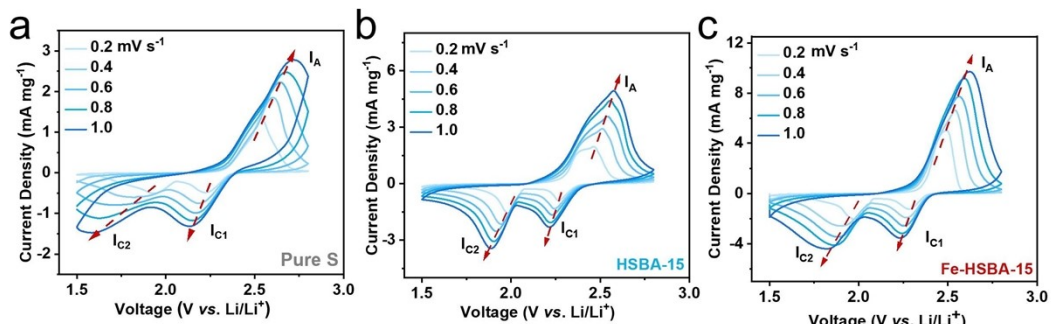


**Fig. S19.** CV curves ( $0.2$  to  $1.0 \text{ mV s}^{-1}$ ) of (a) Pure S, (b) HSBA-15 and (c) Fe-HSBA-15.

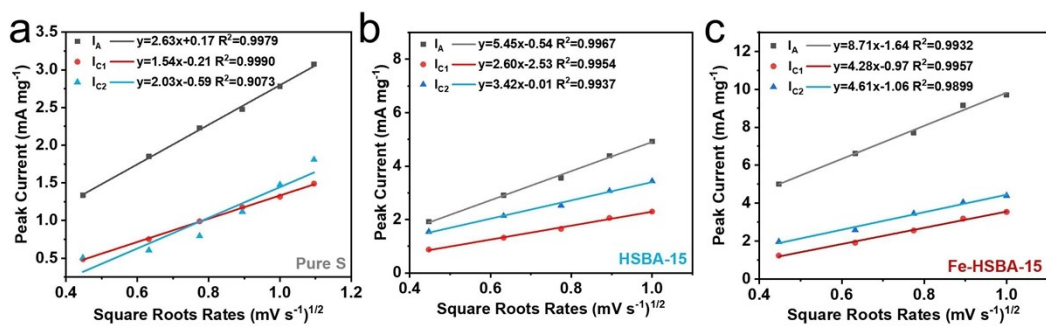


**Fig. S20.** Slope of (a) pure S, (b) HSBA-15/S and (c) Fe-HSBA-15/S.

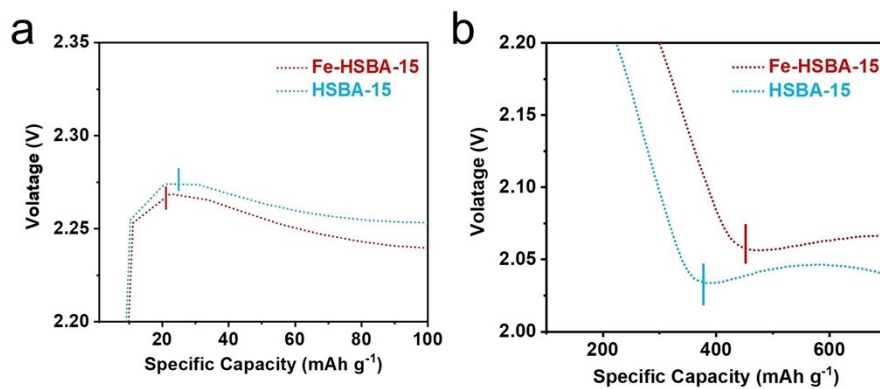


**Fig. S21.** Charge-discharge curves of an enlarged view in (a) 2.20-2.35 V and (b)

2.00-2.20 V with different carrier materials.

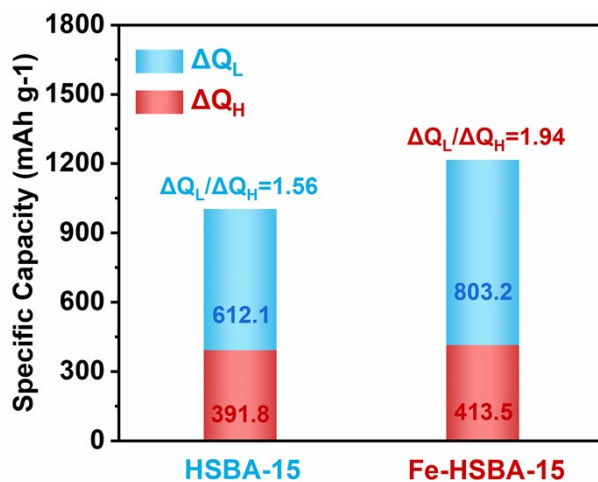


**Fig. S22.**  $\Delta Q_H / \Delta Q_L$  ratios of HSBA-15/S and Fe-HSBA-15/S cathodes.

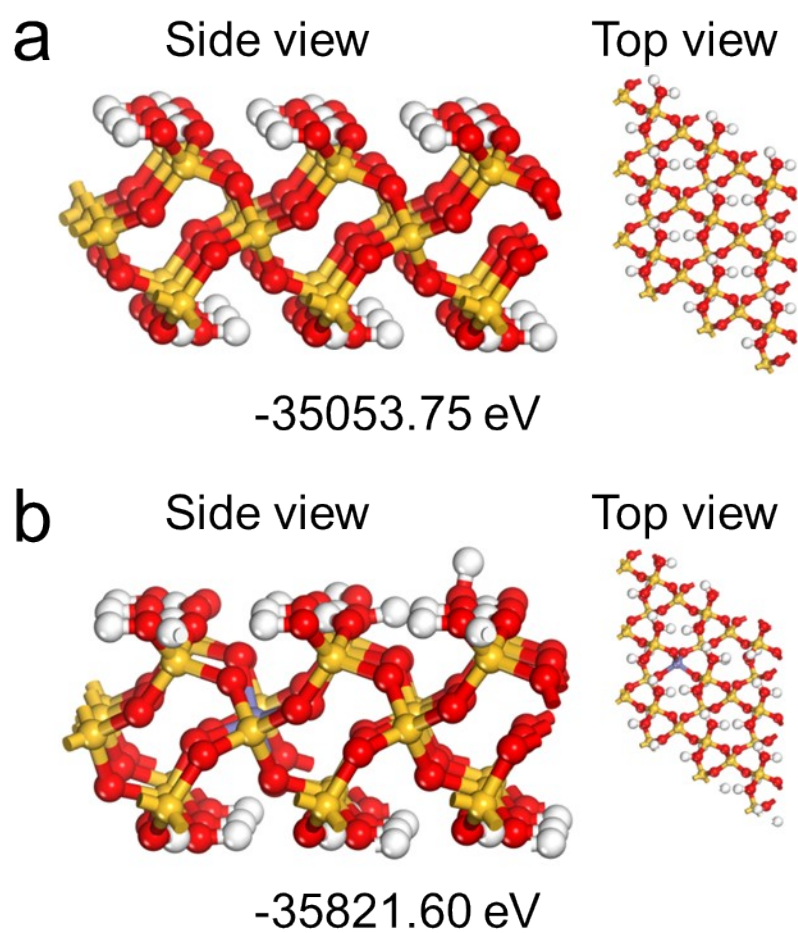


**Fig. S23.** Constructed models and the surface energy of (a) HSBA-15 (b) Fe-

HSBA-15

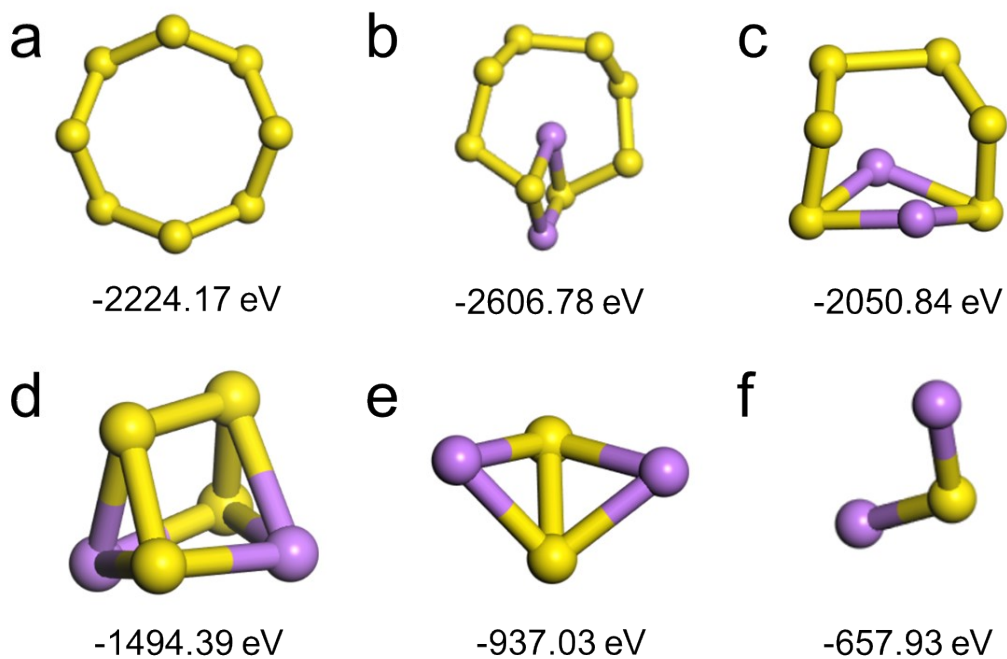


**Fig. S24.** Constructed models and the surface energy of (a)  $S_8$  (b)  $Li_2S_8$  (c)  $Li_2S_6$  (d)  $Li_2S_4$  (e)  $Li_2S_2$  (f)  $Li_2S$

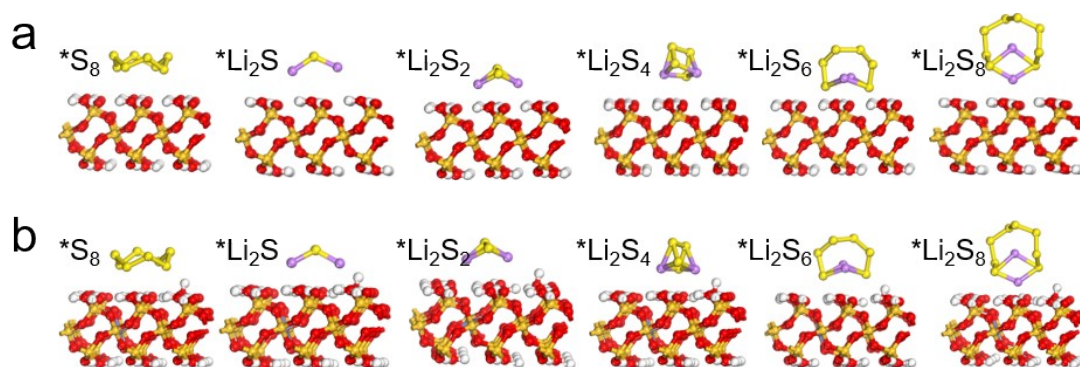


**Fig. S25.** Optimized adsorption configurations of the polysulfides on (a) HSBA-15, (b) Fe-HSBA-15 with the lowest adsorption energy, atom H, O, Si, and Fe are shown as white, red, yellow, and blue, respectively.

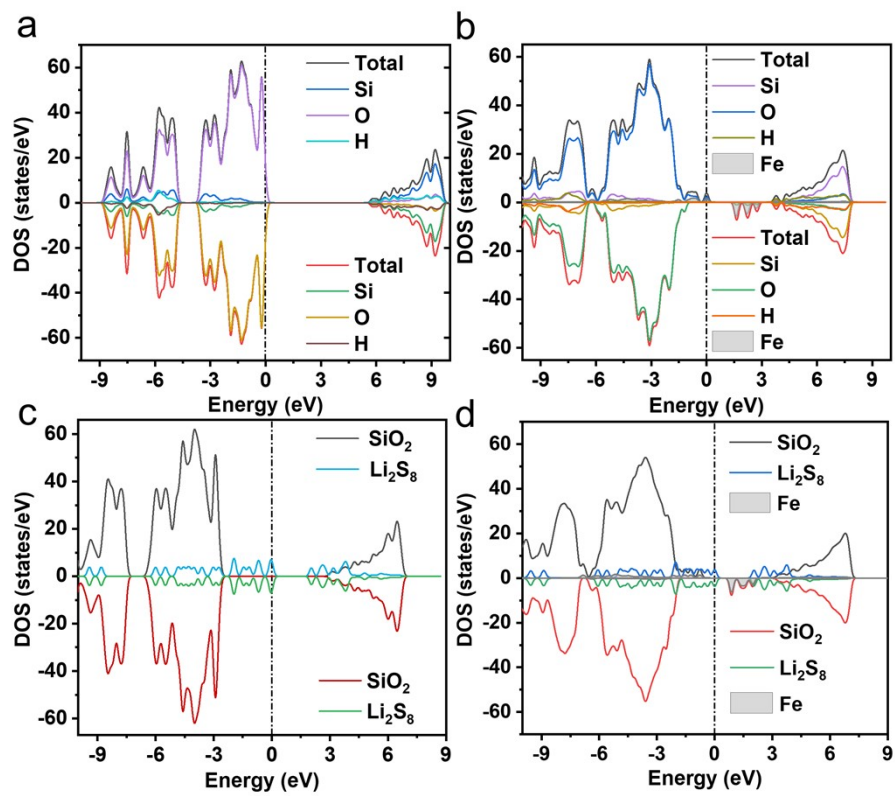


**Fig. S26.** The density of states (DOS) of (a) HSBA-15, (b) Fe-HSBA-15, (c)  $\text{Li}_2\text{S}_8/\text{HSBA-15}$ , (d)  $\text{Li}_2\text{S}_8/\text{Fe-HSBA-15}$ .

## Supporting tables

**Table S1.** ICP results of Fe-HSBA-15 with different HSBA-15 to Fe mass ratio.

Sampel	Sampling quantity [mg]	Iron content [mg kg <sup>-1</sup> ]	Fe mass fraction [wt.%]
Fe-HSBA-15-1	21.5	13241.86	1.32
Fe-HSBA-15-2	22.3	11596.41	1.15
Fe-HSBA-15-3	22.5	9213.33	0.92
Fe-HSBA-15-4	21.9	2675.80	0.27
Fe-HSBA-15-5	23.2	2357.76	0.24

**Table S2.** EIS impedance fitting results of halloysite, HSBA-15 and different ratios of Fe-HSBA-15.

Sampel	$R_S$	$R_{CT}$
Fe-HSBA-15-1	4.99	9.80
Fe-HSBA-15-2	3.44	8.28
Fe-HSBA-15-3	3.53	6.70
Fe-HSBA-15-4	3.28	7.56
Fe-HSBA-15-5	4.37	14.16
Halloysite	8.59	28.06
HSBA-15	3.78	25.11

**Table S3.** BET surface area, average pore Size, and pore volume of Halloysite, HSBA-15 and Fe-HSBA-15 composites.

Sampel	BET surface area [m <sup>2</sup> ·g <sup>-1</sup> ]	Average pore size [nm]	pore volume [cm <sup>3</sup> ·g <sup>-1</sup> ]
Hal	52.80	17.42	0.33
HSBA-15	701.37	6.33	1.11
Fe-HSBA-15-1	683.04	6.38	1.08
Fe-HSBA-15-2	682.99	6.39	1.09
Fe-HSBA-15-3	707.74	6.32	1.12
Fe-HSBA-15-4	705.35	6.25	1.10
Fe-HSBA-15-5	713.50	6.23	1.11

**Table S4.** Electrochemical performance comparison for Li-S coin batteries.

Materials Type	Rate	Areal capacity (mAh·cm <sup>-1</sup> )	Ref.
ZnCoFe-NC/S	1 C	751 (400 <sup>th</sup> )	4
Fe-N	1 C	760 (400 <sup>th</sup> )	5
PNMC-800	1 C	556 (300 <sup>th</sup> )	6
CoP-OMCS	0.5 C	740 (600 <sup>th</sup> )	7
Fe <sub>2</sub> O <sub>3-x</sub> @C@S	2 C	433 (600 <sup>th</sup> )	8
<b>Fe-HSBA-15</b>	<b>1 C</b>	<b>787 (450<sup>th</sup>)</b>	<b>This work</b>

**Table S5.** Zeta potential results of halloysite, HSBA-15 and Fe-HSBA-15 composites.

	Zeta Potential (mV)	Mobility ( $\mu\text{s}/(\text{V}/\text{cm})$ )	Conductance ( $\mu\text{S}$ )	Sample Count Rate (kcps)	Ref. Count Rate (kcps)	RMS Residual
Hal	-16.72	-1.31	34	1182	1818	$1.56 \text{ e}^{-02}$
HSBA-15	-25.97	-2.03	42	1216	1603	$2.62 \text{ e}^{-02}$
Fe-HSBA-15	-58.70	-1.40	102	1707	1968	$1.87 \text{ e}^{-02}$

## Supporting references

- 1 J. P. Perdew, K. Burke M. Ernzerhof, *Physical Review Letters* 1996, **77**, 3865-3868.
- 2 S. Grimme, *J Comput Chem* 2006, **27** (15), 1787-1799.
- 3 J. Furthmüller G. Kresse, *physical Review B* 1996, **54**, 11169-11186.
- 4 X. Zhou, X. Huang, G. Li, P. Zeng, X. Liu, H. Liu, M. Chen Xianyou Wang, *Chemical Engineering Journal* 2023, **471**, 144806.
- 5 X. Hong, L. Kai, Z. Tengfei, L. Xiao, Z. Fanchao, Z. Huifeng, Z. Lirong G. Qiuming, *Chemical Engineering Journal* 2023, **471**, 144553.
- 6 W. Zhao, A. Basem Al, F. Wissam K. Y. S. Ng, *Journal of Electroanalytical Chemistry* 2023, **954**, 118017.
- 7 F. Wang, Y. Han, R. Xu, A. Li, X. Feng, S. Lv, T. Wang, L. Song, J. Li Z. Wei, *Small* 2023, **9**, 2303599.
- 8 J. Pu, Z. Huang, J. Wang, Y. Tan, S. Fan Z. Wang, *Chem Commun (Camb)* 2023, **60** (2), 180-183.